Molecular Orbital Study of Structural Changes on Oxidation and Reduction of S_3, S_4, S_6, and S_8

Dennis R. Salahub,*[1a] Aniko E. Foti,[1b] and Vedene H. Smith, Jr.*[1b]

*Contribution from the Département de Chimie, Université de Montréal,
Montréal, Québec, Canada H3C 3V1, and Department of Chemistry, Queen's University,
Kingston, Ontario, Canada K7L 3N6. Received May 30, 1978*

Abstract: The self-consistent field–$X\alpha$-scattered wave molecular orbital method has been used to provide explanations, in terms of the one-electron orbital energies and wave functions, for the structural changes observed on oxidation and/or reduction of S_3, S_4, S_6, and S_8. The photoelectron and optical spectra are also discussed whenever experimental data are available. For S_3 a Walsh diagram was generated and predicts successively larger bond angles in the series $S_3{}^{2-}$, $S_3{}^-$, S_3. The geometry changes upon successive double reductions of square planar (D_{4h}) $S_4{}^{2+}$ to planar (C_{2v}) S_4 (for which the experimental structure is unknown) and finally to helical (C_2) $S_4{}^{2-}$ are successfully explained. Predictions are made for the likely structural modifications to be expected for the as yet unobserved positive ions of S_6. Reasons are given for the geometry changes in the series: $S_8{}^{4+}$ (as yet unobserved, but analogous to S_4N_4, which has D_{2d} symmetry), $S_8{}^{2+}$ (C_s symmetry), and S_8 (D_{4d} symmetry).

I. Introduction

The elucidation of the structure, the spectra, and other properties of the large number of molecules containing only the atom sulfur presents a definite challenge to modern experimental and theoretical chemistry. In the solid phase more than 30 allotropes of sulfur are known[2] and the liquid and vapor phase consist of extremely complex, temperature- and pressure-dependent mixtures of molecules ranging in size from S_2 up to polymeric species containing about a million atoms.[3] Even if one limits the discussion to species containing ten or fewer atoms, all members of the series S_n, $n = 1$ to 10, have been observed, many of them in more than one oxidation state.[2-33] Beyond their existence, relatively little is known about most of these species. For the neutral molecules, even such a basic property as the geometrical structure is only known for S_2,[29] c-S_6,[30] c-S_7,[31] and c-S_8.[32,33] The electronic structure and binding in these molecules is even less well understood. For instance,[23] as recently as 1974 it was not clear, for the most studied of these molecules, c-S_8, whether the energy levels derived from the sulfur 3s orbitals were in the same energy range as those derived from the 3p orbitals; that is, whether s–p hybridization is significant.

Among the more intriguing recent developments in the field has been the synthesis and characterization, principally by Gillespie and co-workers,[5,17-19,26-28] of a number of polyatomic cations of sulfur and the higher chalcogens, selenium and tellurium. The structures of many of these cations have been determined by X-ray diffraction and are found to be significantly different from those of their neutral counterparts. For example, the well-known crown structure of S_8 is shown in Figure 1a. Removal of two electrons to form $S_8{}^{2+}$ yields the structure shown in Figure 1b. There are two principal differences between these structures. First, the cross-ring S_3–S_7 distance is much shorter in the ion, 286 pm compared with 468 pm in the neutral molecule. Second, in $S_8{}^{2+}$ one of the end sulfurs has flipped to yield an exo,endo conformation whereas the neutral molecule is exo,exo. Similar sensitivity of molecular geometry to oxidation state has been observed for S_4,[13,14] Te_6,[26] a number of "alloy" molecules[27] containing two of the chalcogens, and also some analogous SN compounds.[28]

Understanding of the reasons for these structural changes is rather limited. Gillespie[20,27] has given valence bond structures for a number of cases; however, it is usually necessary to consider contributions from a rather large number of structures, some of which appear to be quite artificial. Another possible approach is that of molecular orbital (MO) theory which could, in principal at least, be applied at several different levels of approximation. At the most sophisticated level, one could envisage carrying out extended basis set Hartree–Fock calculations, complemented where necessary with configuration interaction in order to calculate directly the geometry corresponding to the energy minimum for the molecule and ion in question. The "reasons" for the geometry change would then have to be found by an appropriate analysis, if one can be formulated, of the probably very complicated wave functions involved. For a molecule the size of S_8 this approach appears to be impracticable at present. The only ab initio calculations[35] for neutral S_8 for instance were at the minimum (STO-3G) basis set level. It appears to us unlikely that a lucid explanation of the conformational changes in $S_n{}^{\pm x}$ will result in the foreseeable future from this type of approach.

At the opposite end of the sophistication scale in MO theory lie the empirical and semiempirical methods such as the Extended Hückel (EH)[36] and Complete Neglect of Differential Overlap (CNDO)[37,38] methods. For the present problem, one would probably focus attention not on the total energy but rather on the individual orbital energies and seek the "explanation" of the structural changes by analyzing the geometry dependence of the orbital energies and the simple MO wave functions associated with them. These methods are highly simplified and indeed the results may depend critically on the choice of parameters; however, when used judiciously they have proved to be enormously useful in several different areas of chemistry. The Walsh diagrams[39] which are based on such a scheme have proven predictive ability for the ground and excited state geometries of triatomic molecules. Further examples are found in the Woodward–Hoffmann rules[40] of organic chemistry and the electron counting rules[41,42] used to predict the geometry of borane and transition metal cluster compounds.

In addition to the above traditional quantum chemical methods, in recent years a new molecular orbital method, the Self-Consistent Field–$X\alpha$-Scattered Wave (SCF-$X\alpha$-SW) method[43-45] has been developed. This method shows promise of satisfying to a large extent the desire for a method based on first principles, that is, without a large number of adjustable parameters which may be applied without excessive computational costs, to large molecules, including those with heavier atoms. A number of reviews of the applications of the $X\alpha$ method have been published[46-48] and the reader is referred to these for examples of the utility of this method for a wide variety of applications.

In the present work we have used the $X\alpha$ method to perform calculations on molecules and ions of the series S_3, S_4, S_6, and S_8. Explanations for the geometry changes on oxidation and

reduction are found by analysis of the one-electron MO energy eigenvalues and the corresponding wave functions. In addition, comparison is made with experimental photoelectron and optical spectra whenever the data are available.

In section II we give a short description of the SCF-Xα-SW method and a discussion of the specific advantages of this method for the present type of problem. Section III contains the computational details. The results and discussion for S_3, S_4, S_6, and S_8 respectively are presented in sections IV–VII while the general conclusions and discussion are given in section VIII.

II. Method

All of the results discussed below were obtained with the SCF-Xα-SW method of Slater[43,45] and Johnson.[44] While this method has been thoroughly documented elsewhere, it is sufficiently different from the traditional Linear Combination of Atomic Orbitals Hartree–Fock (LCAO·HF) approach to molecular orbital theory that a brief summary of the more important differences is appropriate here.

The SCF-Xα-SW method is actually a combination of two methods, Slaters's Xα method which yields an approximate one-electron Schrödinger equation and Johnson's scattered wave procedure which allows its solution. The Xα equations may be derived from the Hartree–Fock equations[49] or from the equations for the total energy corresponding to a determinantal wave function,[50,51] by replacing the nonlocal, energy-dependent, exchange-correlation term by a local, average, energy-independent, exchange-correlation term. While this is the manner in which the Xα equations were initially derived, there is growing empirical evidence[52,53] that at least in certain cases Xα results are more accurate than those of the Hartree–Fock approach and that therefore the Xα method contains in a presently incompletely understood manner some of the correlation terms, i.e., that it is capable of going beyond Hartree–Fock theory. The solution to this apparent paradox, an approximation being more accurate than the quantity approximated, may possibly be found in the future through research in density functional theory,[54] and it seems to us a reasonable working hypothesis that the Xα method, rather than being an approximation to HF theory, occupies a roughly equivalent position but in a different formalism.

The one-electron Xα equation is (in Rydberg units, 1 Ry = 13.6058 eV)

$$[-\nabla_1^2 + V_C(1) + (V_{X\alpha\uparrow}(1)]u_{i\uparrow}(1) = \epsilon_i u_{i\uparrow}(1) \qquad (1)$$

where ∇_1^2 is the kinetic energy term, V_C is the coulomb term,

$$V_{X\alpha\uparrow}(1) = -6\alpha \left[\frac{3}{4\pi}\rho^\uparrow(1)\right]^{1/3} \qquad (2)$$

is the exchange potential for an electron of spin up, $\rho^\uparrow(1)$ is the charge density for spin up electrons, α is a scaling factor, $u_{i\uparrow}(1)$ is a spin up molecular orbital, and ϵ_i is the eigenvalue corresponding to u_i. The reasons for the introduction of the parameter α are described in Slater's book.[45] Values of α for all of the atoms have been tabulated by Schwarz.[55]

The solutions to the Xα equations differ in a number of ways from those of the HF method. First, in the Xα method Fermi statistics are satisfied;[45] that is, the energy levels are filled in order of increasing ϵ_i which is not always the case in HF theory because of the exchange terms. The orbital eigenvalues in Xα theory have a different significance from that in HF theory. In HF theory ϵ_{HF} corresponds through Koopmans' theorem[56] to an ionization potential whereas in Xα theory

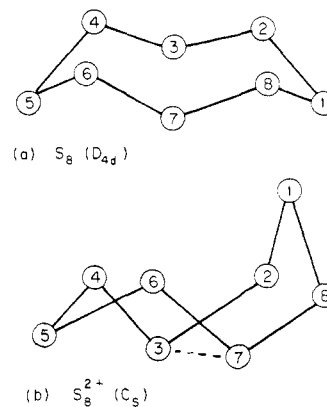$$\epsilon_i = \frac{\partial \langle E_{X\alpha}\rangle}{\partial n_i} \qquad (3)$$

Figure 1. Schematic diagram (a) for the crown-shaped (exo,exo) S_8 and (b) for the doubly positive ion S_8^{2+} (exo,endo). The dashed line between atoms 3 and 7 in (b) indicates that these atoms are closer together than in (a).

where $E_{X\alpha}$ is the statistical total energy and n_i is the occupation number for the ith orbital. Therefore, ϵ_i corresponds to an orbital electronegativity,[57-62] that is, roughly to the average of the ionization potential and the electron affinity for a given orbital. In order to calculate ionization potentials within the Xα theory one may use Slater's transition state method[43] in which one-half of an electron is removed from the orbital in question and the eigenvalue is recalculated self-consistently. Thus a strict comparison of ionization potentials requires a separate calculation for each orbital. However, it often happens that the relaxation energies for orbitals in the valence region are not too different from each other so that a first approximation to the *relative* IP's may be obtained from the unrelaxed orbital energies. For optical transitions, a transition state procedure also exists,[45] in which one removes half an electron from one orbital and places it in another. This yields a multiplet average excitation energy, e.g., average of singlet and triplet energies. To calculate the components separately it is necessary to perform spin-polarized calculations for $\uparrow\uparrow$ and $\uparrow\downarrow$ transition states and take the appropriate average.[63,64]

Another difference between HF and Xα theory which is of prime importance to the present work concerns the unoccupied orbitals. In HF theory the virtual orbitals are calculated in an erroneous N-electron field, wherease in Xα theory all of the orbitals, occupied and virtual, are eigenfunctions of the same potential which corresponds to the proper approximate $N-1$ electron field. In the discussion that follows we will be comparing the relative positions of eigenvalues in molecules containing different numbers of electrons and hence certain orbitals will be occupied in one case and vacant in the other. HF theory or its semiempirical variants such as CNDO would be inadequate for this task.

The second half of the Xα-SW method, the scattered wave method of Johnson,[44] provides solutions of the Xα equations and is the conceptual equivalent of the LCAO part of the LCAO-HF method. In practice, however, it is radically different from the more traditional LCAO approach. In the scattered wave method, space is first divided into spherical regions around the nuclei (collectively called region I), the region outside a large sphere surrounding the entire molecule, region III, and the rest of space, the so-called intersphere region II. A muffin tin potential is constructed, spherically averaged in regions I and III and volume averaged in region II. In regions I and III the wave function is expanded in rapidly convergent series of spherical harmonics and radial wave functions which are determined by *numerical* integration of the radial Schrödinger equation. In region II a multicenter expansion of the wave function is used. Demanding continuity of the wave function and its first derivative across the boundaries of the

Table I. Molecular Geometries Used for the Calculations

molecule	symmetry	bond distance pm	bond distance bohr	bond angles, deg	sphere sizes, bohr		ref
S_3	D_{3h}	198	3.742	60	$R_S = 1.8715$	$R_0 = 3.9810$	75
S_3	C_{2v}	198	3.742	90, 120, 150	$R_S = 1.8715$	$R_0 = 5.6145$	75
S_3	$D_{\infty h}$	198	3.742	180	$R_S = 1.8715$	$R_0 = 5.6145$	75
$S_4{}^{2+}$	D_{4h}	204	3.856	90	$R_S = 1.9282$	$R_0 = 4.6550$	13, 16
S_4	C_{2v}	204	3.856	104	$R_S = 1.9282$	$R_0 = 6.6555$	
$S_4{}^{2-}$	C_2	$\{$203, 207	3.837, 3.913$\}$	104, 76.4	$\{R_S = 1.9185, R_S = 1.9565\}$	$R_0 = 6.6179$	14
S_4	D_{3h}	204	3.856	120	$R_S = 1.9282$	$R_0 = 5.7845$	
S_4	T_d	204	3.856	109.5	$R_S = 1.9282$	$R_0 = 4.2897$	
$Se_4{}^{2+}$	D_{4h}	228	4.310	90	$R_{Se} = 2.1550$	$R_0 = 5.2026$	13
$Te_4{}^{2+}$	D_{4h}	267	5.047	90	$R_{Te} = 2.5236$	$R_0 = 6.1326$	97
S_6	D_{3d}	204	3.851	102.2, 74.5	$R_S = 1.9253$	$R_0 = 6.4484$	30
S_6	C_{2v}	206	3.888	104	$R_S = 1.9442$	$R_0 = 5.5412$	
$S_6{}^{2+}$	C_{2v}	206	3.888	104	$R_S = 1.9442$	$R_0 = 5.5412$	
$S_6{}^{2+}$	C_{2v}	206	3.888	104	$R_S = 1.9442$	$R_0 = 5.5412$	
$S_6{}^{6+}$	D_{3h}	205.675, 205.675	3.8884, 3.8884	60	$R_S = 1.9442$	$R_0 = 4.9141$	
$S_6{}^{6+}$	D_{3h}	205.675, 220.000	3.8884, 4.1588	60	$R_S = 1.9442$	$R_0 = 5.0042$	
$S_6{}^{6+}$	D_{3h}	205.675, 234.305	3.8884, 4.4292	60	$R_S = 1.9442$	$R_0 = 5.0977$	
$S_6{}^{6+}$	D_{3h}	205.675, 249.995	3.8884, 4.7258	60	$R_S = 1.9442$	$R_0 = 5.2035$	
$S_6{}^{6+}$	D_{3h}	205.675, 264.299	3.8884, 4.9962	60	$R_S = 1.9442$	$R_0 = 5.3028$	
$S_6{}^{6+}$	D_{3h}	205.675, 298.176	3.8884, 5.6366	60	$R_S = 1.9442$	$R_0 = 5.5473$	
S_8	D_{4d}	204	3.850	104	$R_S = 1.9253$	$R_0 = 6.4484$	32
S_8	C_s	204	3.850	104.3, 91.5	$R_S = 1.9281$	$R_0 = 7.9215$	20
$S_8{}^{2+}$	C_{2v}	204	3.850	104.3, 91.5	$R_S = 1.9281$	$R_0 = 7.2376$	
$S_8{}^{4+}$	D_{2d}	204	3.850	104	$R_S = 1.9281$	$R_0 = 6.1805$	

system yields a set of energy dependent secular equations which may be solved quite rapidly. The most important distinction between this approach and the LCAO method, apart from the economies of computer time, lies in the nature of the "basis set". In the LCAO approach a fixed set of functions is used to construct all of the MO's whereas in the SW approach the radial functions are found independently for each level and are therefore much more flexible. Roughly speaking a scattered wave calculation which contains spherical harmonics up to a certain maximum l value corresponds to a saturated LCAO basis set of the same l_{max} (e.g., $l_{max} = 1$, the sp limit).

This last advantage of the Xα-SW method is perhaps most apparent in some recent calculations involving transition metal complexes[52,53] where HF calculations show rather large errors, whereas the Xα-SW method furnishes satisfactory results. The reason for this may lie in either or both parts of the Xα-SW method. That is, it may be due to the partial accounting for correlation effects in the Xα part alluded to above, or it may be due to the inadequacy of the necessarily rather restricted sets of d functions used in the LCAO calculations. Further research is clearly needed to determine the contribution of each of these possibilities.

A disadvantage of the Xα-SW procedure in its present form which is relevant to this discussion is that accurate calculations of the total energy cannot be performed economically. The standard programs calculate the total energy for a *charge density* of muffin tin form which is a much more severe approximation than that made by using a muffin tin *potential*. With this procedure bond lengths are typically calculated to be several times too long,[65,66] water is found to be linear,[67] etc. The fault in the total energy calculations lies in the SW part of the method and not in the Xα part since methods which completely avoid the muffin tin approximation, such as the LCAO-Xα[68] and Discrete Variational Xα[69,70] methods, yield reasonable binding curves. Also non-muffin tin corrections can

be made in the Scattered-Wave method via perturbation theory[71-73] and greatly improved results can be obtained. The corrections, however are extremely expensive in terms of computer time and so they do not afford a feasible routine manner of calculating total energies. There is a clear need for an efficient way of using the Xα-SW wave functions, which give every indication of being sufficiently accurate,[74] to calculate binding energies. The above comments on total energy calculations notwithstanding it is possible, as we will show in subsequent sections, to extract useful information concerning variations in molecular geometry from the one electron Xα-SW eigenvalues and eigenfunctions.

III. Details of the Computations

The molecules and symmetries for which calculations were performed were the following: S_3 (D_{3h}, C_{2v}, $D_{\infty h}$), $S_4{}^{2+}$ (D_{4h}, C_{2v}, C_2, D_{3h}), S_4 (T_d, D_{3h}, D_{4h}, C_{2v}, C_2), $S_4{}^{2-}$ (C_2), $S_6{}^{4+}$ (D_{3h}), $S_6{}^{2+}$ (C_{2v}), S_6 (D_{3d}, C_{2v}), $S_8{}^{4+}$ (D_{2d}), $S_8{}^{2+}$ (C_{2v}, C_s), S_8 (D_{4d}), and also $Se_4{}^{2+}$ (D_{4h}) and $Te_4{}^{2+}$ (D_{4h}). Table 1 gives the geometric parameters and the references to the experimental geometry determination where appropriate. Most of the calculations were made using the nonoverlapping sphere, muffin tin, version of the method. The sphere radii used are also shown in Table 1. The effect of allowing the spheres to overlap was examined in a few cases for S_3, S_4, and S_8 by increasing the sphere radii by 30%. This did not change the conclusions regarding the geometries; however the agreement found with observed optical spectra was significantly improved. The details may be found in sections IV, V, and VII.

The value of the exchange parameter α was taken from the compilation of Schwarz[55] and has the value 0.724 75 for all regions of space. In the solution of the secular equations, spherical harmonics up to $l = 1$ were included in the sulfur spheres and up to $l = 2$ on the outer sphere. The effect of adding d partial waves on sulfur was examined for the case of

S_4^{2+} and was found to have negligible effect on the results. The largest contribution of the d functions to any of the occupied or lower vacant orbitals was approximately 10%. The energy gap between occupied e_g and vacant b_{1u} orbitals which give rise to the lowest $\pi^* \leftarrow \pi$ transition changed from 2.44 to 2.41 eV when d functions were added to the overlapping sphere calculation. Therefore, all of the results discussed below include only s and p waves.

Contour plots were generated in the usual manner for most of the orbitals and where appropriate these are presented below either in detail or, to save space, as simplified schematic diagrams which give the sign of the wave function lobes and a rough idea of their spatial extent.

IV. S_3

The structure of neutral S_3 has not been measured although S_3 has been observed in sulfur vapor and liquid. Its ionization potential is known,[8] 9.68 eV, and its absorption[10,11,75] (λ_{max} 430 nm, $\Delta E = 2.9$ eV) contributes to the color of liquid sulfur. The negative ion S_3^- has been observed in alkali halide crystals[9] and also appears to be responsible for the blue color of lapis lazuli and the ultramarines (λ_{max} 625 nm, $\Delta E = 2.0$ eV). S_3^- is bent but the angle is not known. The only S_3 species for which the structure is known[76] is the doubly negative ion S_3^{2-} which has a bond length (hereafter S–S) of 215 pm and an S–S–S angle (hereafter θ) of 103°. For comparison the bond angle in ozone is 117°.

There have only been three previous theoretical studies of S_3 species. Meyer and Spitzer[75] performed extended Hückel calculations for a single geometry, S–S = 198 pm, $\theta = 120°$. They found a gap of 0.92 eV between the highest occupied and the lowest unoccupied molecular orbitals (HOMO–LUMO) which may be compared with the energy of the experimental absorption band of 2.9 eV. Cotton, Harmon, and Hedges[77] perfomed SCF-Xα-SW calculations using overlapping spheres for S_3^- and S_3^{2-}. They found that small variations of S–S did not greatly affect the results of the calculations and so did not vary θ from the assumed value of 110° for S_3^- or the experimental value of 103° for S_3^{2-}. They calculated transition energies for both species and also for S_2^- and concluded that the interpretation of the blue color of lapis lazuli as being due to S_3^- was correct. Carlsen and Schaefer[78] were interested in the possible existence of a low-lying closed (D_{3h}) excited state, analogous to that found for ozone and performed ab initio SCF calculations with a double-ζ basis set. For the open (C_{2v}) form they calculated equilibrium values of 191.9 pm for S–S and 117.5° for θ. However, the SCF calculations find the cyclic form, S–S = 210.6 pm, $\theta = 60°$, to be of lower energy. The authors then argue by analogy with more accurate calculations on O_3 that polarization and correlation effects would reverse this order.

In order to investigate the dependence of the S_3 MO energy eigenvalues on θ we have carried out SCF-Xα-SW calculations on S_3 with θ varying between 60 and 180° in 30° steps. Following Meyer and Spitzer[75] S–S was kept constant at 198 pm and the tangent sphere version of the method was used.

The calculated energy levels separate cleanly into two groups which are derived principally from the s and p atomic orbitals of sulfur respectively. There is only a very slight hybridization, the maximum contribution of s functions in the p band being ~10% and the maximum contribution of p functions in the s band being also ~10%. The energy levels derived from s functions lie between −1.704 Ry and −1.234 Ry while the lowest level of the p band is found at −0.847 Ry. The Walsh diagram for the p band resulting from these calculations is shown in Figure 2 and a schematic representation of the wave functions for $\theta = 60, 120,$ and 180° is given in Figure 3. The HOMO is marked with an X in Figure 2. The part of the diagram between 90 and 180° may be compared with the stan-

dard XY_2 Walsh diagram used by spectroscopists (see ref 79, p 319). Apart from a slight lack of smoothness in the Xα results, caused by the varying volume of the intersphere region as the angle changes, the general features of the two diagrams agree quite well. This part of the diagram can be entirely understood in terms of the following two considerations. First, the slopes of the curves are determined by interactions between the two terminal atoms 1 and 3. If in a given orbital the 1–3 overlap is positive the level descends with decreasing θ and vice versa for negative overlap. Second, these interactions are stronger for σ orbitals than for π orbitals. Starting from the bottom we find the orbitals σ_u, π_u, π_g, π_u, and σ_g for the linear configuration. The σ_u orbital is σ bonding and becomes a b_2 orbital under C_{2v}. It is formally 1–3 antibonding; however, the interaction is weak as most of the density lies along the bonds and hence away from the region between the end atoms. The lower π_u orbital has a large contribution from the central atom and smaller contributions from the end atoms. It is bonding along the S–S bonds and also 1–3 bonding. Deformation to C_{2v} symmetry splits π_u into a $b_1(\pi)$ and an $a_1(\sigma)$ level both of which descend in energy due to the increased 1–3 bonding and as mentioned above the σ orbital descends more rapidly. The π_g orbital is restricted by symmetry to the two end atoms. It is 1–3 antibonding and generates $a_2(\pi)$ and $b_2(\sigma)$ levels under C_{2v}, the first of which is essentially independent of θ while the second increases in energy with decreasing θ (1–3 antibonding). The HOMO of neutral linear S_3 is the π_u level at −0.505 Ry which would contain two electrons yielding an open shell configuration and hence it is improbable that linear S_3 is the ground state. This π_u level is antibonding along S–S bonds but 1–3 bonding. It splits into an $a_1(\sigma)$ and a $b_1(\pi)$ level under C_{2v}. The a_1 level becomes the HOMO and the b_1 level the LUMO for slightly bent S_3. The a_1 level is the most sensitive to θ of all of the levels and descends rapidly as θ decreases until at slightly less than 120° it is no longer the HOMO, having descended below the b_2 level which originated from π_g.

The question of the most favorable angle in the range 90–180° may now be addressed. All of the levels except the upper b_2 level either favor small values or are indifferent to θ. Thus if one starts with linear S_3, θ will first decrease to satisfy the decreasing energy of, principally, the upper a_1 level. At around 120°, however, the b_2 level becomes the HOMO and further decrease in θ raises its energy quite rapidly. Thus a competition is set up and an equilibrium angle somewhat less than 120°, as in the case of ozone, would appear to be the most reasonable.

If one proceeds to smaller angles than 90° in order to examine the closed form of S_3, drastic changes are observed due to the increased 1–3 interactions. Indeed, between 90° and 60° the system changes from a 4π-electron system to a 6π-electron system. This change is most readily understood by considering the vacant $a'_2(\sigma)$ level of cyclic S_3 which becomes a b_2 orbital under C_{2v}. This level is strongly antibonding along all three S–S bonds and opening one of them by increasing θ lowers its energy rapidly so that at $\theta = 90°$ it has changed from an antibonding to an essentially nonbonding orbital and it is more favorable to occupy it than the antibonding $b_1(\pi)$ level. During the opening, charge flows from the central atom to the end atoms to effectively avoid the antibonding interactions along the S–S bonds as illustrated in the third row of Figure 3.

The region between 60 and 90° is characterized by rapid changes in the electronic structure as the atoms 1 and 3 are displaced from a normal S–S bond distance at 60° to $\sqrt{2}$ times this distance at 90°. Beyond 90° the variations are much slower and, as described above, correspond essentially to lone pair–lone pair interactions which are adequately accounted for in the one-electron Walsh diagram treatment. It is clear, however, that the orbital energy criterion cannot answer the question of whether the closed or the open form of S_3 is more stable and
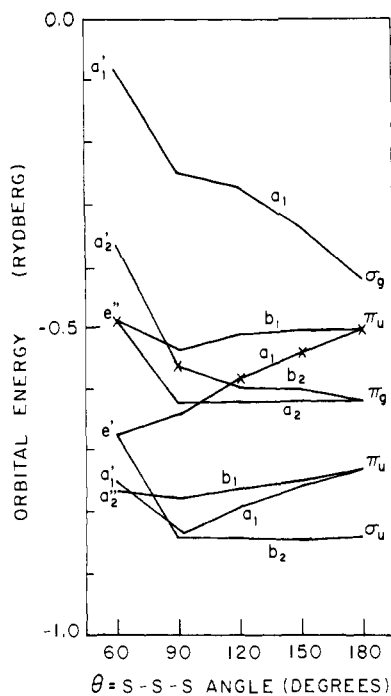
Figure 2. $X\alpha$ Walsh diagram for S_3: molecular orbital eigenvalues (Rydbergs (Ry = 13.6058 eV)) as a function of bond angle (degrees).

Figure 3. Schematic diagram for the one-electron orbital wave functions of S_3 for θ = 60, 120, and 180°. The orbitals are not shown in energetic order for the 60° column but rather are aligned with the C_{2v} orbital to which they correspond. The orbital energies may be found in Figure 2. For degenerate orbitals both symmetry components of the orbital are given. The π orbitals are designated by circles. The size of the orbitals is approximately in proportion to the calculated atomic charges. Black indicates positive and white negative values of wave function.

Figure 4. Orbital eigenvalues (Rydbergs (Ry = 13.6058 eV)) for S_3, θ = 120°: (a) (MT) muffin tin touching sphere calculation; (b) overlapping sphere (OS) (30% increase) calculation.

by how much. This must await more accurate calculations. The Walsh diagram can, however, provide information about the central theme of this paper, namely, what happens to the geometry if one changes the number of electrons.

If one starts with the cyclic (ground or low-lying excited state) geometry and forms a negative ion by adding one or two electrons, these will enter the a'_2 level which can be greatly stabilized by opening the ring. Thus the Walsh diagram definitely predicts an open geometry for S_3^- and S_3^{2-}. The only experimental data is for the S_3^{2-} ion which has two electrons in the $b_1(\pi)$ level and has a bond angle of 103°. Removal of electrons from this 1–3 bonding orbital would result in an opening of the angle consistent with the estimate of Cotton et al.[77] of 110° for the angle in S_3^- and the above estimate of roughly 120° for S_3.

Finally we wish to discuss the spectroscopic data for neutral S_3. Only two data are available. Berkowitz and Lipschitz[8] reported the ionization potential of S_3 as 9.68 eV and Meyer et al.[10,11,75] reported an absorption band at 430 nm, i.e., a transition energy of 2.9 eV. It is often found in $X\alpha$-SW calculations that spectroscopic data are better interpreted, especially for planar molecules, if one increases the sphere radii and allows overlap.[66,80] We have therefore carried out an additional calculation for θ = 120° in which the radii were increased by 30%. The effect of overlap on the orbital eigenvalues is shown in Figure 4 where the p band eigenvalues for the two calculations are plotted. As usual, the overlapping sphere calculation yields a somewhat wider band; however, the same ordering of the energy levels results. The HOMO–LUMO gap increases from 0.94 to 1.24 eV. The ionization potentials corresponding to removal of an electron from the upper a_1, b_2, and a_2 orbitals were calculated using Slater's transition state method. The values 9.45 eV (a_1), 9.68 eV (b_2), and 9.70 eV (a_2) were found in excellent agreement with the experimental value of 9.68 eV for the ionization threshold. It is also noteworthy (Figure 2) that only in the vicinity of θ = 120° are the top three levels so close together. Thus a photoelectron spectrum coupled with our results would provide quite conclusive geometrical information. Moreover, on the basis of the energy level patterns shown in Figure 2, the cyclic and open forms of
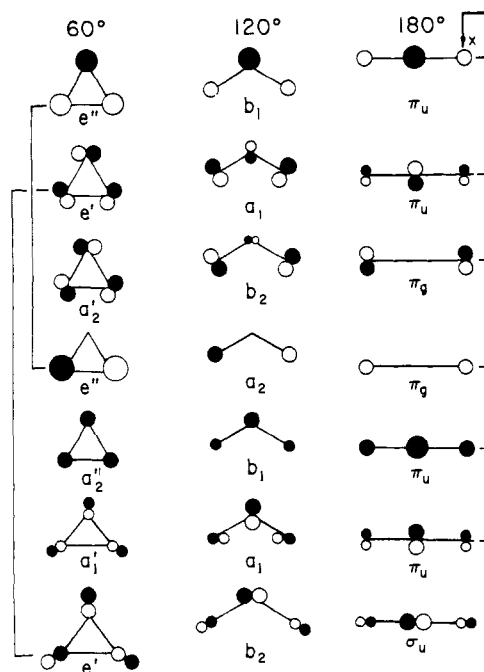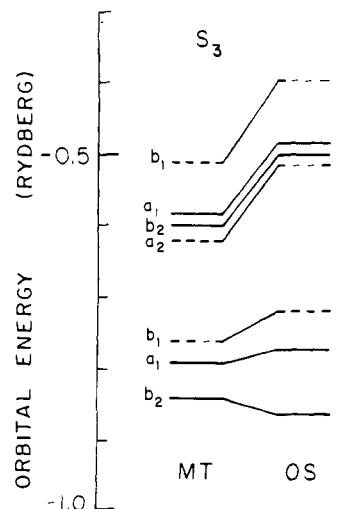
S_3 would have radically different photoelectron spectra so that a clear-cut choice could be made. It might be possible to separate the photoelectron signal of S_3 in the complex mixture present in sulfur vapor by varying the temperature and correlating intensity variations with those of the optical absorption band at 430 nm.

Transition state energies were also calculated for the excitation of an electron from the a_1, b_2, and a_2 orbitals to the vacant b_1 orbital. Spin-polarized calculations were performed in order to calculate the spin-allowed singlet–singlet transition energies. The excitation energies found were 1.52 eV ($b_1 \leftarrow a_1$, $^1B_1 \leftarrow {}^1A_1$), 1.71 eV ($b_1 \leftarrow b_2$, $^1A_2 \leftarrow {}^1A_1$), and 1.97 eV ($b_1 \leftarrow a_2$, $^1B_2 \leftarrow {}^1A_1$). The transition to $^1A_2$ is symmetry forbidden. Also,
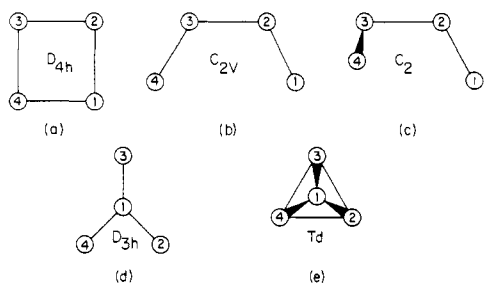
Figure 5. Molecular conformations for S_4: (a) square planar (D_{4h}); (b) open planar, (C_{2v}); (c) nonplanar (C_2); (d) planar branched (D_{3h}); (e) tetrahedral (T_d).

previous detailed calculations for ozone[63] have indicated that the molecular orbital method is intrinsically incapable of adequately describing certain highly polar excited states of which the $^1B_2$ state in ozone analogous to that above is an example. In ozone this state was calculated at 2.99 eV by the $X\alpha$-SW method whereas the most accurate Generalized Valence Bond-Configuration Interaction calculations put it at 6.93 eV.[81-85] Thus the only spin- and symmetry-allowed single-electron transition expected in the visible region is that calculated at 1.52 eV ($^1B_2 \leftarrow {}^1A_1$) to which we assign the observed broad band with a maximum at 2.9 eV. The agreement is adequate, considering that the exact geometry in neither the ground nor the excited state is known. According to the Walsh diagram, closing the angle somewhat would tend to increase the energy of this transition.

V. S_4

Like neutral S_3, the structure of neutral S_4 is not known, and also like S_3 an absorption band[10,11,75] in the visible region (ΔE = 2.3 eV) contributes to the color of liquid sulfur. Unlike S_3, it has not yet proven possible to measure the ionization potential of S_4. Two S_4 ions have been reasonably well characterized. S_4^{2+} has the square (D_{4h}) structure[13,16] shown in Figure 5a. The bond length has not been measured, but consideration of the analogous Se_4^{2+} and Te_4^{2+} ions leads one to expect only small changes from normal S—S bond lengths. We have used the value 204 pm whenever other values were not available from experiment. S_4^{2+} has a pale yellow color[16] due to an abosorption band at 330 nm (ΔE = 3.8 eV), the tail of which reaches into the visible. The doubly negative ion S_4^{2-} has the nonplanar, C_2 structure[14] shown in Figure 5c. The bond length is 207 pm, the SSS angle is 104°, and the dihedral angle is 76.4°. The proximity of the bond length to the normal SS bond length (206 ppm in c-S_8) indicates that the two extra electrons are in essentially S–S nonbonding orbitals. This structure is similar[86] to that of one form of the iso-(valence-electronic) molecule S_2F_2.

There is a paucity of theoretical work on S_4, only four papers in addition to a preliminary account[87] of the present work being relevant. In 1968, Brown et al.[13] pointed out, on the basis of simple Hückel reasoning, that Se_4^{2+} (and hence S_4^{2+}) with 22 electrons would have a closed shell configuration in a square-planar geometry but not in linear or tetrahedral conformations. Meyer and Spitzer[75] performed extended Hückel calculations for a number of conformations of neutral S_4. Their lowest energy conformation was the branched (D_{3h}) trithio-sulfur trioxide form; however, recent ab initio calculations by Kao,[88] at the 44-31 G level, find this configuration to be the least stable among all of the geometries considered. Kao finds the ground state to be a triplet of helical geometry although it is not clear whether or not this is an artefact of the method which usually favors triplet states unduly; e.g., the ground state of ozone[63,81-85] is erroneously predicted to be a triplet by the Hartree-Fock method. The $X\alpha$ method correctly predicts a
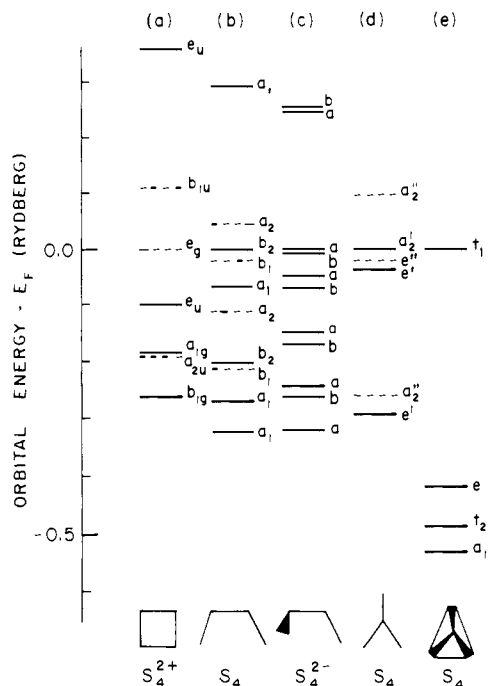

Figure 6. Orbital eigenvalues (Rydbergs (Ry = 13.6058 eV)) relative to the Fermi level for: (a) S_4^{2+} (D_{4h}) symmetry; (b) S_4 (C_{2v} symmetry); (c) S_4^{2-} (C_2 symmetry); (d) S_4 (D_{3h} symmetry); (e) S_4 (T_d symmetry). The t_1 level of T_d is only occupied by four electrons. Dashed lines indicate π orbitals.

singlet ground state for ozone.[63] Even if one restricts the discussion to singlet states, geometry predictions based on ab initio Hartree-Fock calculations can be quite sensitive to the basis set used and also correlation effects may be important. A relevant example may be found in the Hartree-Fock calculations of Carlsen and Schaefer[78] for S_3 mentioned in the last section. The only other relevant theoretical work is a molecular mechanics study[89] which found that c-S_4 would be highly strained. A fair assessment of the situation is that one does not appear to be able at this stage to calculate the ground state geometry of S_4 with any degree of confidence and our results presented below do not purport to do this. Nevertheless much insight into the dependence of geometry on oxidation state can be gained from approximate calculations as we will now show.

We have examined the five configurations shown in Figure 5. The relevant orbital energy diagrams are shown in Figure 6. In this figure, since species of different charge are being compared each column has been uniformly shifted in order to align the Fermi levels. For a number of the ions involved, S_4^{2+} (D_{4h}), S_4^{2+} (C_{2v}), S_4^{2+} (C_2), S_4^{2+} (D_{3h}), and S_4^{2-} (C_2), we have also performed calculations for the corresponding neutral molecules in order to test whether the relative positions of the levels for a given geometry are sensitive to the gain or loss of two electrons. They are not. If one aligns the Fermi level of either molecule with its counterpart in the ion the maximum difference between corresponding levels of the occupied p band is $\sim$0.07 eV; thus the same ordering and relative spacing of the levels are found independent of the charge. The calculated Fermi levels for neutral molecules in the geometries of columns a to e are -0.434, -0.657, -0.605, -0.582, and -0.312 Ry, respectively.

Column e of Figure 6 shows the results for the tetrahedral geometry which has an open-shell electronic configuration, the Fermi level being of t_1 symmetry and containing four electrons. Thus this geometry may be safely ruled out as the ground state of S_4. The above is consistent with the known[90] tetrahedral structure of P_4 which contains four fewer electrons and would therefore yield a closed shell electronic configuration.

Column d of Figure 6 shows the energy levels for the D_{3h}, trithiosulfur trioxide geometry. A closed shell configuration is found and without an accurate total energy calculation this geometry cannot be eliminated as a candidate for the ground state of S_4. The analogy with sulfur trioxide along with EH calculations has been invoked[75] to favor the stability of this conformation; however, as mentioned above the ab initio calculations find it to be the least stable of all those geometries which were considered. Once again, the photoelectron spectrum of S_4, if it could be measured, would allow a clear-cut choice between the D_{3h} geometry and the C_{2v} geometry shown in column b which as we argue below is also a reasonable possibility for the ground state. For the D_{3h} geometry there are three levels clustered near the Fermi level and then a wide gap on the high binding energy side. On the other hand, the C_{2v} molecule has a much more even distribution of levels throughout the p band.

We will restrict the remaining discussion to the three cases shown in columns a to c which form a reasonable series starting with square planar S_4^{2+} (col. a) and leading to nonplanar S_4^{2-} (column c).

Column b represents an intermediate open planar (C_{2v}) geometry which our calculations indicate may be a likely candidate for the geometry of the lowest singlet state of neutral S_4. We will now give an explanation for the structural changes in terms of the positions of the energy levels and the character of their associated wave functions. S_4^{2+} is found to be a closed shell system with an orbital eigenvalue spectrum very similar[91,92] to that of S_2N_2 with which it is iso-(valence-electronic) and isostructural. The similarity is even more striking if one examines the wave functions. One of the interesting features of SN compounds is that the net charge transfer from sulfur to nitrogen is close to 0.5 electron so that each ends up with about 5.5 valence electrons. This is reflected in the individual orbitals, either individually or taken in pairs, by rather uniform distribution of the electrons between S and N so that contour diagrams are quite similar to those of homonuclear molecules. Comparison of Figure 7b below with Figure 5 of ref 92 will illustrate this point. The HOMO–LUMO gap for S_4^{2+} is about 1.5 eV so that gain of electrons in this geometrical configuration to yield neutral S_4 would be unfavorable, the LUMO being an antibonding π orbital.

Let us now focus our attention on column b of Figure 6 which corresponds to an open planar C_{2v} conformation in which one of the S–S bonds has been stretched. This perturbs the energy levels of column a to various degrees. By far the most drastic change occurs for the virtual e_u level of the D_{4h} configuration which decreases in energy (relative to E_F) by more than 4.5 eV and becomes the Fermi level (b_2) for the neutral C_{2v} molecule. The b_{1u} virtual level of the D_{4h} geometry also falls somewhat and for S_4^0 (C_{2v}) the HOMO–LUMO gap becomes 0.55 eV. Thus one can see that opening the square would facilitate the reduction of S_4^{2+} to S_4^0.

A completely analogous situation has previously been discussed[91] for the opening of S_2N_2. In this case the σ level analogous to $b_2(\sigma)$ actually falls very slightly below but nearly degenerate with the equivalent of the $b_1(\pi)$ level. Since there are two less electrons in S_2N_2 than in S_4 this was argued to lead in all likelihood to a reactive open shell species and subsequently by interaction with another such species to the generation of the conducting polymer $(SN)_x$. In S_4, however, both of these levels are filled and the LUMO is 0.55 eV higher (or even more in an overlapping sphere calculation, see below) so that a stable singlet in this geometry is quite feasible. In support of the feasibility of this geometry we mention that the analogous molecule S_2O_2 is of exactly this configuration, surprisingly so according to Steudel.[4] Also a molybdenum complex[93] containing S_4 as a σ-bonded ligand is known and a planar arrangement of the sulfurs has not been ruled out. The presence

(o)   (c)
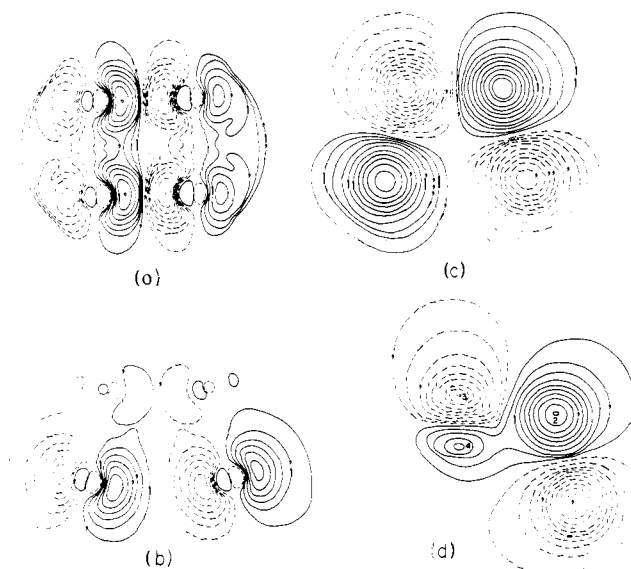
(b)   (d)

Figure 7. Contour plots for selected molecular orbital wave functions: (a) the e_u virtual level of S_4^{2+} (D_{4h}), Figure 5a, (b) the b_2 (Fermi) level of S_4 (C_{2v}), Figure 5b; (c) the a_2 virtual level of S_4 (C_{2v}), Figure 5b; and (d) the a (Fermi) level of S_4^{2-} (C_2), Figure 5c. (a) and (b) are plotted in the molecular plane and (c) and (d) in a plane 1 bohr above the S–S–S plane. Dashed contours indicate negative values of the wave function. The outermost contour has the values 0.02282, 0.03371, 0.00840, and 0.01849 au for a, b, c, and d, respectively. Adjacent contours differ by 0.02237, 0.03300, 0.00823, and 0.01812 au respectively for a, b, c, and d.

of σ bonding in this complex is consistent with the energy position and wave-function character (see below) of the $b_2(\sigma)$ level which we find as the HOMO of S_4 (C_{2v}).

Next let us consider the transition from the C_{2v} to the C_2 structure. Here the changes are more subtle than in the previous deformation. The major effect near the Fermi level of the out-of-plane deformation is to lower the relative energy of the a_2 level of the C_{2v} conformation. For the helical geometry one finds two close-lying occupied orbitals (a and b) at the Fermi level. There is a very large HOMO–LUMO gap (3.4 eV) consistent with the stability of S_4^{2-} in this geometry. Thus by following the positions of the orbital eigenvalues one can see that stretching one S–S bond in S_4^{2+} allows the facile gain of two electrons to form S_4 and the out-of-plane deformation facilitates the gain of yet two more electrons to yield the closed shell S_4^{2-}.

The reasons for the changes in orbital eigenvalue position may be ascertained by examining the corresponding wave functions. Figure 7a shows a contour diagram of the wave function for one component of the virtual e_u orbital of S_4^{2+}. The important aspect of this figure for our purposes is the antibonding nature of this orbital along the bottom S–S bond of the square. When this bond is stretched to yield the C_{2v} geometry, the b_2 (Fermi) level shown in Figure 7b results. Clearly the stretching of the S–S bond has "relieved" the antibonding nature of the orbital, hence the dramatic drop in orbital energy. It is also interesting that in the b_2 orbital charge is concentrated on the end atoms, effectively avoiding the antibonding region along the unstretched upper S–S bond.

For the $C_{2v} \rightarrow C_2$ deformation, as mentioned above, the orbital energy shifts are more subtle. Nevertheless the principal reason for the shifts and the consequent acceptance of two electrons to form S_4^{2-} may be isolated. Since an out-of-plane deformation is involved one might expect involvement of the π electrons of the C_{2v} geometry and indeed this is the case. Figure 7c shows the a_2 virtual level of the C_{2v} geometry in a plane 1 bohr (52.9177 pm) above the atoms. This orbital is antibonding with respect to all of the S–S bonds. On going to the C_2 geometry the σ–π distinction no longer exists and indeed
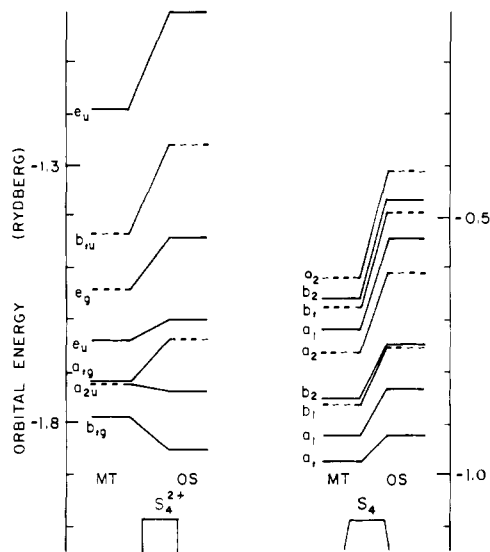
Figure 8. Orbital energies: (a) S_4^{2+} (D_{4h}) from (MT) muffin tin touching sphere and (OS) overlapping sphere calculation; (b) S_4 (C_{2v}) from (MT) and (OS) calculations.

the orbitals receive contributions from both σ and π levels of the C_{2v} geometry. The $a_2(C_{2v})$ level contributes primarily to the $a(C_2)$ level, i.e., the Fermi level of S_4^{2-}. A plot of this orbital also in a plane 1 bohr above the plane of three atoms is shown in Figure 7d. The orbital is still antibonding along the S–S bonds but now the positive lobes of the p functions on atoms 2 and 4 are closer to each other and a bonding overlap results accounting for the increased stability of this orbital in the C_2 geometry.

Finally we wish to discuss the spectroscopic data on S_4^{2+}, its analogues Se_4^{2+} and Te_4^{2+}, and also neutral S_4. Absorption spectroscopy and magnetic circular dichroism[6] studies on S_4^{2+}, Se_4^{2+}, and Te_4^{2+} have yielded bands at 3.8, 3.0, and 2.4 eV, respectively. The lowest transition according to the calculations should be from the occupied e_g level, which corresponds to sulfur π lone pairs, to the π antibonding level of b_{1u} symmetry. The difference in orbital energy is respectively 1.46, 1.21, and 0.92 eV for the S, Se, and Te ions; thus the observed red shift on going to the heavier elements is successfully accounted for. In order for a more exact comparison with experiment to be made we have performed a transition state calculation which also yielded a value of 1.46 eV for S_4^{2+} corresponding to an average of singlet–singlet and singlet–triplet transition energies. Thus the transition energy in the muffin tin calculations is somewhat too low. This behavior has previously been noted for nonoverlapping sphere calculations and as seen for S_3 in section IV may be remedied by increasing the sphere sizes. We have therefore made a calculation in which the sulfur sphere radii were increased by 30%. The effect of overlapping the spheres on the orbital eigenvalues is illustrated in Figure 8 and is qualitatively similar to the behavior already discussed for S_3. Spin-polarized transition-state calculations were made in order to separate the singlet and triplet energies. These yielded a singlet–triplet $b_{1u} \leftarrow e_g$ transition at 2.26 eV and the corresponding symmetry-allowed singlet–singlet transition at 2.56 eV in the visible region and in quite reasonable agreement with experiment considering that the precise geometries in the ground and excited states are not known.

For neutral S_4 an absorption band is observed at 530 nm $(\Delta E = 2.3 \text{ eV})$. We have calculated singlet–singlet transition energies for the orbital transitions $(a_2 \leftarrow b_2)$ and $(a_2 \leftarrow b_1)$ which are both symmetry allowed, and are found at 0.88 and 1.12 eV, respectively. Considering the uncertainty in the exact geometrical parameters, the agreement with experiment is ade-
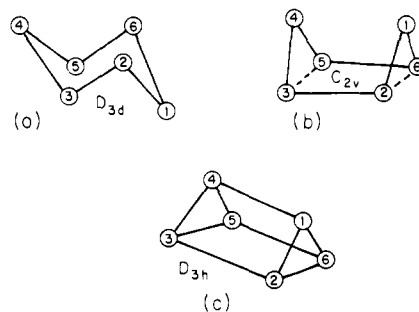

Figure 9. Molecular conformations of S_6: (a) chair form (D_{3d}); (b) boat (C_{2v}); (c) equilateral prism (D_{3h}).

quate and accounts satisfactorily for the red shift observed on going from S_4^{2+} to S_4.

VI. S_6

Relatively little experimental information is available on the $S_6^{\pm x}$ system and hence this section will be somewhat more speculative than the previous two sections on S_3 and S_4 and the next section on S_8. The only S_6 species which has been characterized is the neutral S_6 molecule which is present in the rhombohedral allotrope of solid sulfur also known as Engel's sulfur and Aten's sulfur. The S_6 molecule has the chair configuration[30] shown in Figure 9a. Its ionization potential[8] is 9.00 eV. The absorption spectrum of S_6 in ethyl ether above 250 nm has been reported[10] and consists of a very long tail extending from 250 nm to beyond 400 nm into the visible region. No distinct maxima are observed although there appears to be a shoulder at about 280 nm $(\Delta E \approx 4.4 \text{ eV})$.

No ions of S_6 have so far been identified but very recently Gillespie and co-workers[26,27] have synthesized a number of six-atom ions involving various combinations of sulfur and the higher chalcogens. The ions $Te_3S_3^{2+}$ and $Te_2Se_4^{2+}$ have the boat configuration shown schematically in Figure 9b with apparently one cross-ring bond. The Te_6^{4+} cation has the equilateral trigonal prism structure shown in Figure 9c and it has been speculated that the as yet unknown species Te_6^{6+} would have the same type of structure but with a shorter distance between the two triangular faces of the prism.

Thus for this six-atom system there is a large number of geometries which can be formed through angular and bond length changes. These can be conveniently classified as follows starting from the chair configuration of S_6 (Figure 9a). Flipping S_1 up yields the boat conformer shown in Figure 9b. Bringing atoms 1 and 4 closer together yields a triangular prism in which the faces have an SSS angle of 104°. We will refer to this geometry as an isosceles prism. Formation of a cross-ring bond in each end of the prism yields equilateral triangular faces (equilateral prism). Finally moving the triangular faces of the prism further from each other yields the long equilateral prism shown in Figure 9c. Clearly, the determination of the optimum structure for each charge state of $S_6^{\pm x}$ would be a gargantuan task and we do not pretend to have accomplished this. However, we do believe that the calculations and the discussion given below provide insight which taken together with future experimental work on the positive S_6 ions will lead to a better understanding of the reasons for the structural changes accompanying oxidation and reduction in this series.

We will start the discussion with the equilateral short prism which has been suggested to be the structure of Te_6^{6+} and by extension of S_6^{6+}. We reiterate that this structure has not been observed and must therefore be regarded only as a reasonable working hypothesis. Other as yet unconsidered structures may turn out to be the ground state of S_6^{6+}; for instance, the trigonal prism can be deformed into an octahedron with only
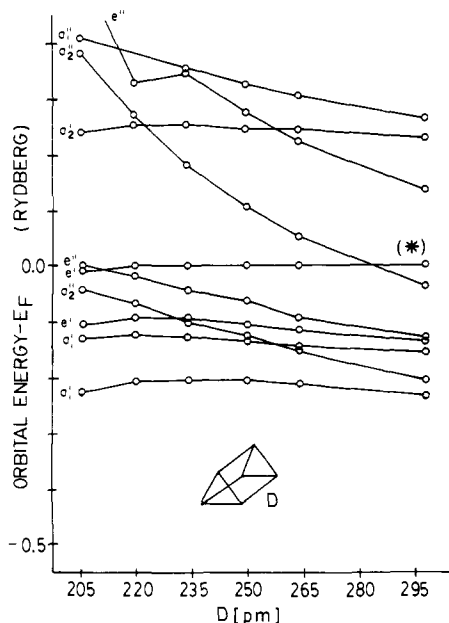
Figure 10. Correlation diagram for S_6^{6+} ions. Orbital energies (Rydbergs) relative to the Fermi level (E_F) of S_6^{6+} (see text) as a function of D (pm). The Fermi levels for D = 205.675, 221.000, 234.305, 249.995, 264.299, and 298.176 are -2.5995 Ry, -2.5681 Ry, -2.4998 Ry, -2.4277 Ry, -2.3706 Ry, and -2.2360 Ry, respectively. Note that in the last column at D = 298.176 pm the Fermi level e' is occupied by only two electrons.

quite small displacements of the atoms so that an octahedral structure should likely be retained as a possibility.

Accepting, for the moment, that the short equilateral prism is the structure of S_6^{6+} we wish to determine whether deformations of the structure which would facilitate the reduction to S_6^{4+}, S_6^{2+}, and finally to neutral S_6 can be found, tracked in terms of the energy level positions, and understood in terms of the orbital wave functions.

In Figure 10 we show our results in the form of a correlation diagram for the equilateral prism in which the length of the rectangular faces has been varied from the normal S–S bond distance of 206 pm at the left to a long prism value of 299 pm which corresponds to the long distance found in Te_6^{4+} (310 pm) multiplied by the ratio of normal S–S and Te–Te bond lengths. The zero of energy has been aligned for each calculation with the energy level corresponding to the Fermi level of S_6^{6+} (i.e., 18 p electrons). The calculations were performed for S_6^{4+}; however, as seen above for S_4 the relative positions will not change greatly with charge state and this will not affect the qualitative arguments given below. The values of the S_6^{6+} Fermi level and the corresponding values of D, the length of the rectangular faces, are given at the bottom of the figure.

We will consider first the short prism whose eigenvalues are at the left of Figure 10. There is a large HOMO–LUMO gap of 3.26 eV between the occupied e'' level and the vacant a'$_2$ level and this would bode well for the stability of S_6^{6+} in this geometry. If we now wish to reduce S_6^{6+} to S_6^{4+} it would seem likely that some geometrical deformation would exist to lower one or more of the virtual levels relative to the occupied levels. Indeed, as Figure 10 shows if one simply pulls the two ends of the prism apart the virtual a''$_2$ level descends rapidly, and in fact at large enough distance (about 280 pm) descends below the e' level. A contour plot for this level at D = 234.3 pm, in the plane containing atoms 2, 3, 5, and 6, is shown in Figure 11 and clearly illustrates the antibonding nature of this orbital between the triangular faces and thus the decrease in orbital energy may be understood. Thus a long prism analogous to that of Te_6^{4+} seems a reasonable candidate for the structure of S_6^{4+}, at least a better candidate than the short prism. Further discussion of this particular set of calculations is probably
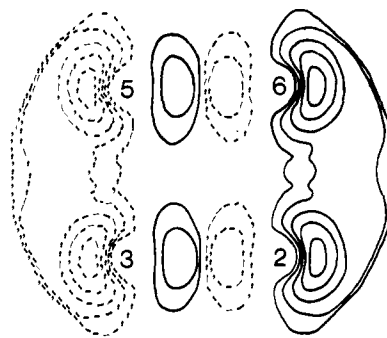

Figure 11. Contour plot for the a''$_2$ virtual level (see text) of S_6^{4+} (D_{3h}) at D = 234.305 pm. The wave function is plotted in the plane of atoms 2, 3, 5, and 6 (see Figure 9c). Dashed contours indicate negative values of the wave function. The outermost contour has the value 0.01547 au. Adjacent contours differ by 0.01517 au.
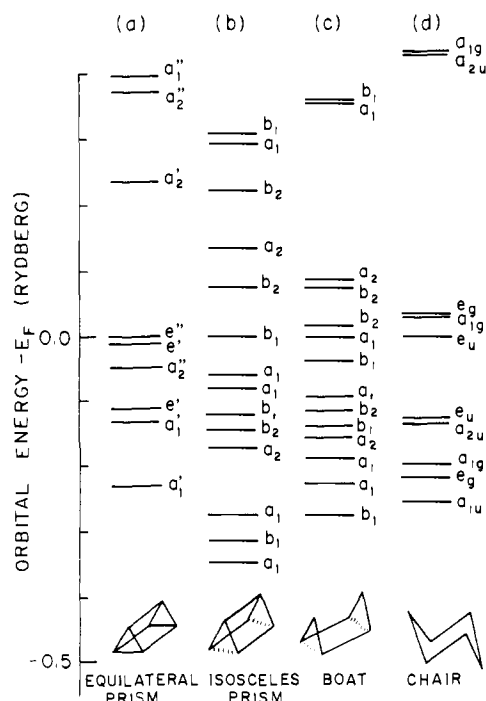

Figure 12. Orbital energies (Rydbergs) for S_6 molecules and ions referred to the Fermi level (E_F) corresponding to S_6^{6+} for (a) the equilateral prism, (b) the isosceles prism, (c) the boat, and (d) the chair. The actual charge state used in the calculations was +4, +2, +2, and 0 for (a), (b), (c), and (d), respectively (see text).

unjustified in view of the lack of experimental data. Future experimental advances may justify their revival.

We now consider a different type of deformation of the short equilateral prism, namely an increase of one of the SSS angles in each of the triangular faces from 60° to a normal SSS angle of 104°, i.e., to form the isosceles prism. The energy level diagrams for the two prisms are shown in Figure 12, columns a and b, referred to the Fermi level of S_6^{6+}. This deformation, like the previous one, has a relative stabilizing influence on some of the virtual levels and indeed three of them, b$_2$, a$_2$, and a second b$_2$, are found below the position of the a''$_2$ (LUMO) of the equilateral prism. So this is another way to facilitate the gain of electrons. This structure, if the b$_2$ and a$_2$ levels were occupied, corresponds to S_6^{2+} and is quite similar to the structures of the "alloy" ions $Te_3S_3^{2+}$ and $Te_2Se_4^{2+}$ mentioned above. Further deformation of the isosceles prism to the boat, Figure 12, column c, and finally the chair conformation, column d, causes a further descent of these levels until finally in the chair the e$_g$ and a$_{1g}$ levels which will contain the six elec-
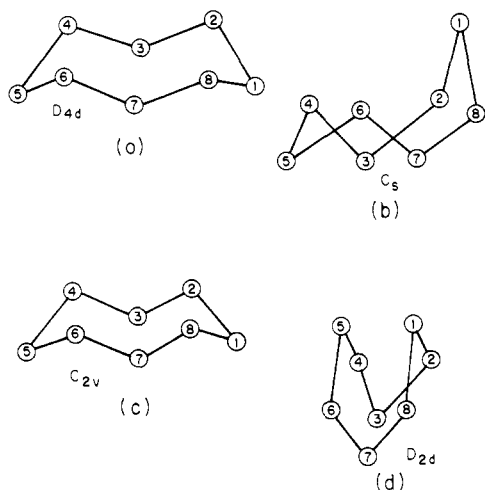
Figure 13. Molecular conformations of S_8: (a) crown shape (D_{4d}), (b) exo,endo (C_s); (c) exo,exo (C_{2v}); and (d) endo,endo (D_{2d}).

trons needed to form a neutral molecule are both within 0.43 eV of the e_u level (the Fermi level for S_6^{6+} in the chair conformation). The HOMO–LUMO gap for the chair form of S_6 is 5.38 eV consistent with its stability.

To conclude this section we will discuss the limited amount of spectroscopic data available for neutral S_6. A transition state calculation for ionization from the e_g (HOMO) yields a value of 9.40 eV in good agreement with the experimental threshold of 9.0 eV. Thus for this quite closely packed molecule it appears that the nonoverlapping sphere version of the method is adequate. For the optical transitions, as mentioned above, the HUMO–LUMO gap is 5.38 eV and the corresponding singlet–singlet transition would have an even greater energy. This is considerably larger than the energy corresponding to the shoulder observed at 4.4 eV in the spectrum[10] of a solution of S_6 in ethanol. Neither the concentration nor the absolute value of the absorbance was given for this solution so it is difficult to judge the significance of the shoulder. Also, since the occupied orbitals involved in the lower transitions are essentially sulfur lone pairs the possibility of complexing or at least some association with the solvent cannot be ruled out. Further experimental work on the S_6 spectrum is clearly needed before a meaningful comparison can be made with the calculations.

VII. S_8

The neutral S_8 molecule is the best characterized of all of the species discussed in this paper. Its structure has been determined by X-ray diffraction[32,33] and the familiar crown shape (D_{4d}) is shown in Figure 13a. Its photoelectron spectrum has been measured in both the solid[23,25] and gaseous[21,24] states with ultraviolet and X-ray photons and is discussed below. The absorption spectrum of S_8 in solution and in a glass has been reported.[10] Two peaks near 270 nm $(\Delta E \approx 4.6$ eV) are observed and have been assigned[94] to an $E_1 \leftarrow A_1$ transition presumably split by the Jahn–Teller effect. Thus, interestingly, at low temperature S_8 is colorless; the familiar yellow color arises from vibrational hot bands. The reflectivity of orthorhombic sulfur has also been measured[22] and indicates that the first optical transition should be near 4 eV.

The only molecular ion of S_8 which has so far been characterized[17-20] is the doubly positive S_8^{2+} species which has the (C_s) structure shown in Figure 13b. As mentioned in the Introduction there are two principal differences between this structure and the D_{4d} structure of S_8, namely, the short cross-ring bond (S_3-S_7) and the exo,endo, rather than exo,exo, conformation. S_8^{2+} is blue due to a broad absorption band centered at 590 nm $(\Delta E \approx 2.1$ eV).

It is also interesting to note that although the ion S_8^{4+} has not yet been made, it would be iso-(valence-electronic) with S_4N_4 which has the endo,endo structure[95] shown in Figure 13d with two short cross-ring $S\cdots S$ bonds. S_4N_4 has been the subject a previous study[91] using the SCF-Xα-SW method and the above $S\cdots S$ interaction shows up clearly in the contour plots of several MO's shown in that paper. We have made a calculation for S_8^{4+} in the D_{2d} geometry of S_4N_4 and the results are discussed below along with those for S_8^{2+} and neutral S_8.

There have been a number of previous theoretical studies of neutral S_8. The extended Hückel method has been used by several authors[21,23,75] and with a suitable choice of parameters it is possible to obtain reasonable values for the ionization potential and the first transition energy. It is found[23] that 3d orbitals do not contribute significantly to the occupied orbitals and also that sp hybridization is minor, indicating that the use of sp^3 hybrids as the starting point is inappropriate. S_8 has also been studied by the molecular mechanics method[89] where it was used to help define the force field parameters. SCF-Xα-SW calculations were performed on S_8 by Richardson and Weinberger;[24] however, there appears to be an error in these calculations as we have found different results (see below). Our results were checked by doing the calculations twice, using two independent versions of the Xα-SW program, and complete agreement was found. Also, several inadequacies of the previous Xα-SW results were pointed out by Salaneck et al.[25] who performed CNDO calculations for S_8 in order to interpret the photoelectron spectrum. Our new Xα-SW results are in quite good agreement with the results of Salaneck et al. as far as the ordering and overall spacing of the levels is concerned. A few close-lying levels are interchanged in the two calculations. We have previously reported[74] Xα-SW calculations for the electronic deformation density of S_8 which showed that satisfactory agreement for this extremely sensitive property could be obtained if a sufficiently large set of partial waves was included in the calculations. New Xα-SW results for the photoelectron and optical spectra of S_8 have been reported and discussed by Foti, Smith, and Connolly.[96] Finally we mention that a minimum basis set (STO-3G) ab initio calculation has been performed[35] for S_8. An energy minimum was found quite close to the observed structure.

We turn now to our results and the question of the differing geometries of S_8, S_8^{2+}, and S_8^{4+} for which we assume D_{2d} symmetry. Once again, our arguments are clearer if we start from the most positive species and search for deformations which will decrease the orbital energy of a virtual level and thereby facilitate the gain of electrons, although the reverse order of reasoning is clearly equivalent.

The calculated eigenvalues relative to the Fermi level corresponding to S_8^{4+} (28 p electrons) for the four geometries shown in Figure 13 are given in Figure 14. Column a shows the results for the D_{2d} geometry (S_8^{4+}). The eigenvalue spectrum is extremely similar to that found in Xα calculations for S_4N_4 (see Figure 1 of ref 90). There is a somewhat greater amount of sp hybridization for S_4N_4 than for S_8^{4+} which leads to a slight overlap of the "s" and "p" bands in the former. However, for the present discussion of geometry changes upon reduction it is the region near the Fermi level which is important and in this respect the two molecules are essentially alike. In particular, for both there is a large HOMO–LUMO gap (2.5 eV for S_4N_4 and 1.26 eV for S_8^{4+}) consistent with their stability (observed for S_4N_4, assumed for S_8^{4+}) in this geometry.

In order to facilitate the double reduction of S_8^{4+} to S_8^{2+} one may change the conformation from endo,endo (Figure 13d) to endo,exo (Figure 13b). The principal effect of this change is to separate S_1 and S_5. A contour plot of the virtual e level of S_8^{4+} in a plane containing these two atoms is shown in Figure 15 which clearly shows that this orbital is S_1-S_5 antibonding. Separating S_1 and S_5 lowers the symmetry to C_s
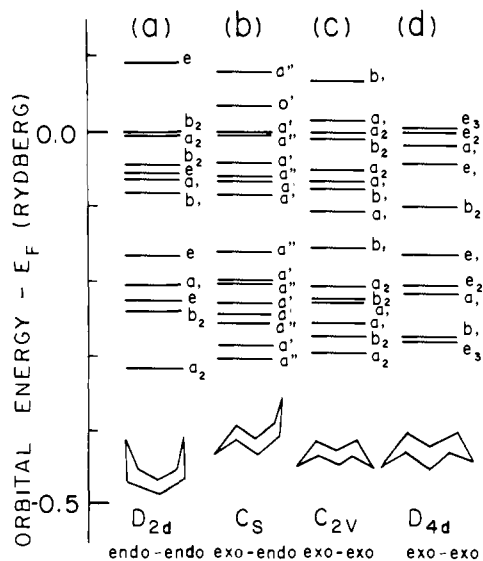
Figure 14. Orbital energies (Rydbergs) for S_8 molecules and ions referred to the Fermi level (E_F) corresponding to S_8^{4+} for (a) the endo,endo (D_{2d}), (b) the exo,endo (C_s), (c) the exo,exo (C_{2v}), and (d) the exo,exo (D_{4d}). The actual charge state used in the calculations was +4, +2, +2, and 0 for (a), (b), (c), and (d), respectively (see text).

Figure 15. Contour plot for the e virtual level (see text) of S_8^{4+} (D_{2d}). Figure 13d. The wave function is plotted in a plane containing the atoms S_1 and S_5 and parallel to that containing atoms 4, 6, 2, and 8. Dashed contours indicate negative values of the wave function. The outermost contour has the value of 0.01255 au. Adjacent contours differ by 0.01230 au.

Figure 16. Contour plot for the a″ virtual level (see text) of S_8^{2+} (C_s), Figure 1b. The wave function is plotted in the plane of atoms 3, 7, 2, and 8. Dashed contours indicate negative values of the wave function. The outermost contour has the value 0.02640 au. Adjacent contours differ by 0.0259 au.

and the e level splits into an a′ and an a″ level. The a′ level descends significantly in energy owing to the decreased antibonding interaction as shown in column b of Figure 14 so that in the C_s geometry observed for S_8^{2+} it is only 0.48 eV above the S_8^{4+} Fermi level. Thus the endo,endo to endo,exo deformation allows a more facile gain of two electrons. We turn now to an examination of the observed structural differences between S_8^{2+} (C_s) and neutral S_8 (D_{4d}).

The eigenvalues for these two cases, still relative to the Fermi level corresponding to S_8^{4+}, are given in columns b and d, respectively, of Figure 14. In S_8^{2+} the a′ level shown at +0.035 Ry is occupied while the a″ level at +0.081 Ry is vacant, i.e., a HOMO–LUMO gap of 0.62 eV. After deformation to the D_{4d} geometry of neutral S_8 this gap has been reduced to essentially zero, and therefore the gain of two electrons should be easier. The principal reason for the descent of the a″ level has been isolated and is illustrated in Figure 16 which shows a contour plot of this orbital in a plane containing the atoms S_3 and S_7 which are involved in the cross-ring bond in S_8^{2+}. The a″ orbital is antibonding between these two atoms so that moving them further apart decreases its orbital eigenvalue. Thus the breaking of the S_3···S_7 partial bond on going from S_8^{2+} to S_8, or equivalently its formation upon ionization of S_8 to S_8^{2+}, may be understood. The deformation discussed immediately above actually consists of both the lengthening of the S_3–S_7 distance and a conformational change from exo,endo to exo,exo. In order to examine the effects of these two changes separately we have made an additional calculation for the C_{2v} geometry (Figure 13c) in which the S_3–S_7 distance is left at its short value as in S_8^{2+}, but the exo,exo conformation (as in neutral S_8) is adopted. The results of this calculation are shown in column c of Figure 14. Comparing columns b and c we can evaluate the effects of flipping one end of the molecule. These effects turn out to be relatively minor, and in particular the HOMO–LUMO gap for S_8^{2+} is essentially unchanged. Thus the change in the S_3–S_7 distance is far more important in the reduction of S_8^{2+} to S_8 than is the change from exo,endo to exo,exo conformations. The differences between these latter conformations are subtle and explanations for the preference of a particular species for one or the other must await future detailed total energy calculations.

We turn now briefly to the $X\alpha$ results for the spectroscopic data for the S_8 species, which are discussed in some detail
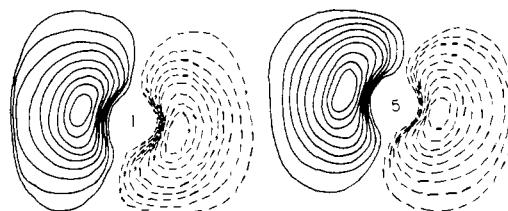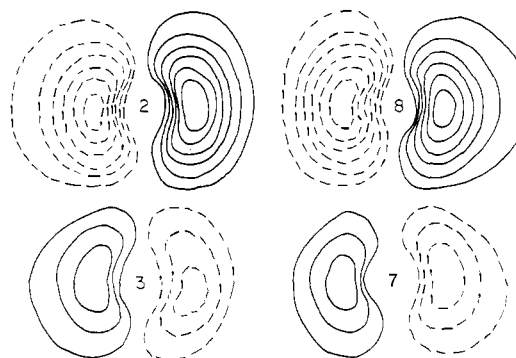
elsewhere.[96] Figure 17 shows the experimental photoelectron spectrum, the CNDO results,[24] and our $X\alpha$-SW muffin tin results which were calculated by the transition state method. The calculated first IP is 8.50 eV in excellent agreement with the experimental value. The p band is calculated significantly too narrow; however, the overall agreement as to the ordering and the general pattern of the levels is satisfactory and permits essentially the same assignments of the peaks as found by Salaneck et al.[25] In order to examine the effect of overlapping spheres (OS) on the spectrum we have made a calculation in which the sphere radii were increased by 30%. The results of this calculation are also presented in Figure 17. As expected the p band width increases significantly compared with the muffin tin results. Full details are given elsewhere.[96]

We have made transition state calculations for the singlet–singlet transitions of S_8 corresponding to the orbital excitations ($b_2 \leftarrow a_1$), ($e_3 \leftarrow e_2$), ($b_2 \leftarrow e_3$), and ($e_3 \leftarrow e_1$) which are the only four symmetry-allowed transitions resulting from excitation from one of the four uppermost occupied levels to the two lowest virtual levels. For the two transitions involving two degenerate levels the results quoted below do not correspond to pure symmetry eigenfunctions and are therefore more approximate than the other two values. These four singlet–singlet transitions are calculated to be at 4.38, 4.22, 4.51, and 5.11 eV, respectively, in good agreement with the experimental absorption maximum at 4.6 eV. The presence of four allowed transitions in this energy range is also consistent with the results of CNDO calculations.[25]

VIII. Conclusion

In each of the cases discussed above we have sought to explain the structural changes which accompany oxidation or reduction of a molecule in the S_n series by examining the one-electron energies and wave functions calculated with the
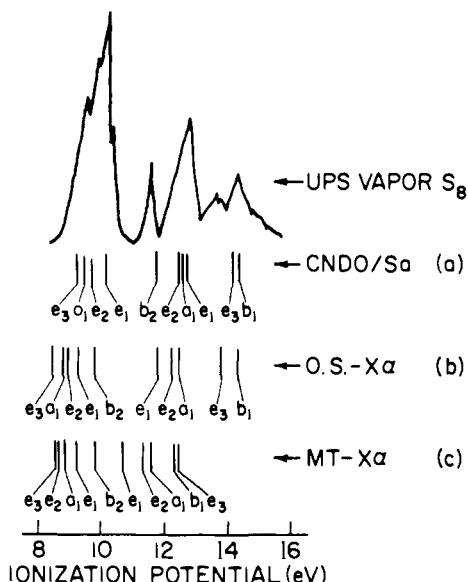
Figure 17. UPS data for S_8 (from ref 20) are shown at the top. The vertical lines indicate in (a) the positions in energy of the molecular orbitals of the p band from ref 24, in (b) the calculated ionization potentials for the overlapping sphere (OS) calculations. Only the uppermost e_3 and a_1 levels were calculated by the transition state method. The other levels were obtained by shifting the orbital eigenvalues by 2.32 eV which is the average of the relaxation shift for the e_3 (2.33 eV) and a_1 (2.31 eV) levels, and in (c) calculated transition state ionization potentials for the muffin tin (MT) calculation.

SCF-$X\alpha$-SW method. In each case when two molecules differing by two electrons were compared the most positive member of the pair always possessed a virtual level which was antibonding between two (or more) sulfur atoms. A structural deformation which increased the distance between these two atoms was isolated and this deformation led to a stabilization of the virtual level and consequently to the more facile reduction of the molecule in the deformed geometry. This reasoning can of course be reversed, that is to say that oxidation of the molecule containing the larger number of electrons removes a certain amount of antibonding character between the atoms in question and allows them to approach each other.

The present treatment has entirely ignored total energy considerations for the basic reason that at the present time the total energy cannot be accurately and economically calculated within the framework of the $X\alpha$-SW method or for that matter, as far as molecules of this size are concerned, by any method. There is a great need for an accurate and efficient algorithm for the $X\alpha$-SW total energy and we hope that in the future we will be able to supplement the one-electron arguments given above with values of the total energy for the various geometries involved. We are confident that the lucid and physically appealing explanations we have given above contain the essence of the physics of these fascinating structural changes.

References and Notes

(1) (a) Université de Montréal; (b) Queen's University.
(2) B. Meyer, *Chem. Rev.*, **64**, 429 (1964); **76**, 367 (1976).
(3) M. Schmidt, *Angew. Chem., Int. Ed. Engl.*, **12**, 445 (1973).
(4) R. Steudel, *Angew. Chem., Int. Ed. Engl.*, **14**, 655 (1975).
(5) R. J. Gillespie and J. Passmore, *Acc. Chem. Res.*, **4**, 413 (1971).
(6) J. Schneider, B. Dischler, and A. Räuber, *Phys. Status Solidi*, **13**, 141 (1966).
(7) J. Suwalski and H. Seidel, *Phys. Status Solidi*, **13**, 159 (1966).
(8) J. Berkowitz and C. Lipschitz, *J. Chem. Phys.*, **48**, 4346 (1968).
(9) W. Holzer, W. F. Murphy, and H. J. Bernstein, *J. Mol. Spectrosc.*, **32**, 13 (1969).
(10) B. Meyer, T. V. Oommen, and D. Jensen, *J. Phys. Chem.*, **75**, 912 (1971).
(11) B. Meyer, T. Stroyer-Hansen, and T. V. Oommen, *J. Mol. Spectrosc.*, **42**, 335 (1972).
(12) F. P. Daly and C. W. Brown, *J. Phys. Chem.*, **77**, 1859 (1973).
(13) I. D. Brown, D. B. Crump, R. J. Gillespie, and D. P. Santry, *J. Chem. Soc., Chem. Commun.*, 853 (1968).
(14) S. C. Abrahams and J. L. Bernstein, *Acta. Crystallogr., Sect. B*, **25**, 2365 (1969).
(15) A. T. Ward, *Mater. Res. Bull.*, **4**, 581 (1969).
(16) P. J. Stephens, *J. Chem. Soc., Chem. Commun.*, 1496 (1969).
(17) R. J. Gillespie, J. Passmore, P. K. Ummat, and O. C. Vaidya, *Inorg. Chem.*, **10**, 1327 (1971).
(18) R. J. Gillespie and P. K. Ummat, *Inorg. Chem.*, **11**, 1674 (1972).
(19) R. J. Gillespie and J. Passmore, *J. Chem. Soc., Chem. Commun.*, 1333 (1969).
(20) C. G. Davies, R. J. Gillespie, J. J. Park, and J. Passmore, *Inorg. Chem.*, **10**, 2781 (1971).
(21) R. Boschi and W. Schmidt, *Inorg. Nucl. Chem. Lett.*, **9**, 643 (1973).
(22) B. E. Cook and W. E. Spear, *J. Phys. Chem. Solids*, **30**, 1125 (1969).
(23) P. Nielsen, *Phys. Rev. B*, **10**, 1673 (1974).
(24) N. V. Richardson and P. Weinberger, *J. Electron Spectrosc. Relat. Phenom.*, **6**, 109 (1975).
(25) (a) W. R. Salaneck, N. O. Lipari, A. Paton, R. Zallen, and K. S. Liang, *Phys. Rev. B*, **12**, 1493 (1975); (b) W. R. Salaneck, C. B. Duke, A. Paton, and C. Griffiths, *ibid.*, **15**, 1100 (1977).
(26) R. J. Gillespie, W. Luk, and D. R. Slim, *J. Chem. Soc., Chem. Commun.*, 791 (1976).
(27) R. J. Gillespie, W. Luk, E. Maharajh, and D. R. Slim, *Inorg. Chem.*, **16**, 892 (1977).
(28) R. J. Gillespie, D. R. Slim, and J. D. Tyrer, *J. Chem. Soc., Chem. Commun.*, 253 (1977).
(29) G. Herzberg, "Molecular Spectra and Molecular Structure", Vol. I, Van Nostrand, Princeton, N.J., 1950.
(30) J. Donohue and A. Caron, *J. Am. Chem. Soc.*, **83**, 3748 (1961).
(31) I. Kawada and E. Hellner, *Angew. Chem., Int. Ed. Engl.*, **9**, 379 (1970).
(32) S. C. Abrahams, *Acta Crystallogr.*, **8**, 661 (1955); **14**, 311 (1961); **18**, 566 (1965).
(33) A. Caron and J. Donohue, *Acta Crystallogr.*, **18**, 562 (1965).
(34) R. Gleiter, *J. Chem. Soc. A*, 3174 (1970).
(35) G. L. Carlson and L. G. Pedersen, *J. Chem. Phys.*, **62**, 4567 (1975).
(36) R. Hoffmann, *J. Chem. Phys.*, **39**, 1397 (1963).
(37) J. A. Pople, D. P. Santry, and G. A. Segal, *J. Chem. Phys.*, **43**, S129 (1965).
(38) J. A. Pople and G. A. Segal, *J. Chem. Phys.*, **43**, S136 (1965).
(39) A. D. Walsh, *J. Chem. Soc.*, 2260, 2266, 2288, 2296, 2301, 2306 (1953).
(40) R. B. Woodward and R. Hoffmann, *J. Am. Chem. Soc.*, **87**, 395, 2046, 2511 (1965); *Angew. Chem., Int. Ed. Engl.*, **8**, 781 (1969).
(41) K. Wade, *Chem. Br.*, **11**, 177 (1975); *New Scientist*, 615 (June 6, 1974).
(42) D. M. P. Mingos, *Nature (London)*, *Phys. Sci.*, **236**, 99 (1972).
(43) J. C. Slater, *Adv. Quantum Chem.*, **6**, 1 (1972), and references therein.
(44) K. H. Johnson, *Adv. Quantum Chem.*, **7**, 143 (1973), and references therein.
(45) J. C. Slater, "The Self-Consistent Field for Molecules and Solids", Vol. 4, McGraw-Hill, New York, N.Y., 1974.
(46) K. H. Johnson, *Annu. Rev. Phys. Chem.*, **26**, 39 (1975).
(47) R. P. Messmer in "Modern Theoretical Chemistry", Vol. 8, G. A. Segal, Ed., Plenum Press, New York, N.Y., 1977, p 215.
(48) N. Rösch in "Electrons in Finite and Infinite Structures", P. Phariseau, Ed., Plenum Press, New York, N.Y., 1977.
(49) J. C. Slater, *Phys. Rev.*, **81**, 385 (1951).
(50) R. Gaspar, *Acta. Phys. Acad. Sci. Hung.*, **3**, 263 (1954).
(51) W. Kohn and L. J. Sham, *Phys. Rev.*, **140**, A1133 (1965).
(52) E.g., F. A. Cotton and G. G. Stanley, *Inorg. Chem.*, **16**, 2668 (1977).
(53) E.g., D. R. Salahub, *J. Chem. Soc., Chem. Commun.*, 385 (1978).
(54) P. Hohenberg and W. Kohn, *Phys. Rev.*, **136**, B864 (1964).
(55) K. Schwarz, *Phys. Rev. B*, **5**, 2466 (1972).
(56) T. Koopmans, *Physica (Utrecht)*, **1**, 104 (1933).
(57) R. S. Mulliken, *J. Chem. Phys.*, **46**, 497 (1949).
(58) R. P. Iczkowski and J. L. Margrave, *J. Am. Chem. Soc.*, **83**, 3547 (1961).
(59) J. Hinze and H. H. Jaffé, *J. Am. Chem. Soc.*, **84**, 540 (1962).
(60) J. Hinze, M. A. Whitehead, and H. H. Jaffé, *J. Am. Chem. Soc.*, **85**, 148 (1963).
(61) G. Klopman, *J. Am. Chem. Soc.*, **86**, 1463 (1964).
(62) K. H. Johnson, *Int. J. Quantum Chem., Symp.*, **11**, 39 (1977).
(63) R. P. Messmer and D. R. Salahub, *J. Chem. Phys.*, **65**, 779 (1976).
(64) T. Ziegler, A. Rauk, and E. J. Baerends, *Theor. Chim. Acta*, **43**, 261 (1977).
(65) P. Weinberger and D. D. Konowalow, *Int. J. Quantum Chem., Symp.*, **7**, 353 (1973).
(66) D. R. Salahub, R. P. Messmer, and K. H. Johnson, *Mol. Phys.*, **31**, 529 (1976).
(67) U. Mitzdorf, *Theor. Chim. Acta*, **37**, 129 (1975).
(68) H. Sambe and R. H. Felton, *J. Chem. Phys.*, **62**, 1122 (1975).
(69) E. J. Baerends, D. E. Ellis, and P. Ros, *Chem. Phys.*, **2**, 41 (1973).
(70) E. J. Baerends and P. Ros, *Chem. Phys.*, **2**, 52 (1973).
(71) J. B. Danese and J. W. D. Connolly, *J. Chem. Phys.*, **61**, 3063 (1974).
(72) J. B. Danese, *J. Chem. Phys.*, **61**, 3071 (1974).
(73) J. B. Danese, *Chem. Phys. Lett.*, **45**, 150 (1977).
(74) D. R. Salahub, A. E. Foti, and V. H. Smith, Jr., *J. Am. Chem. Soc.*, **99**, 8067 (1977).
(75) B. Meyer and K. Spitzer, *J. Phys. Chem.*, **76**, 2274 (1972).
(76) S. C. Abrahams, *Acta Crystallogr.*, **7**, 432 (1954).
(77) F. A. Cotton, J. B. Harmon, and R. M. Hedges, *J. Am. Chem. Soc.*, **98**, 1417 (1976).

(78) N. R. Carlsen and H. F. Schaefer, *Chem. Phys. Lett.*, **48**, 390 (1977).
(79) G. Herzberg, "Molecular Spectra and Molecular Structure III. Electronic Spectra and Electronic Structure of Polyatomic Molecules", Van Nostrand-Reinhold, New York, N.Y., 1966.
(80) F. Herman, A. R. Williams, and K. H. Johnson, *J. Chem. Phys.*, **61**, 3508 (1974).
(81) P. J. Hay and W. A. Goddard III, *Chem. Phys. Lett.*, **14**, 46 (1972).
(82) P. J. Hay, T. H. Dunning, Jr., and W. A. Goddard III, *Chem. Phys. Lett.*, **23**, 457 (1973).
(83) W. A. Goddard III, T. H. Dunning, Jr., W. J. Hunt, and P. J. Hay, *Acc. Chem. Res.*, **6**, 368 (1973).
(84) P. J. Hay, T. H. Dunning, Jr., and W. A. Goddard III, *J. Chem. Phys.*, **62**, 3912 (1975).
(84) W. A. Goddard III, P. J. Hay, and T. H. Dunning, to be published.
(86) R. L. Kuczkowski, *J. Am. Chem. Soc.*, **86**, 3617 (1964).

(87) A. E. Foti, V. H. Smith, Jr., and D. R. Salahub, *Chem. Phys. Lett.*, **57**, 33 (1978).
(88) J. Kao, *Inorg. Chem.*, **16**, 2085 (1977).
(89) J. Kao and N. L. Allinger, *Inorg. Chem.*, **16**, 35 (1977).
(90) F. A. Cotton and G. Wilkinson, "Advanced Inorganic Chemistry", Wiley-Interscience, New York, N.Y., 1966.
(91) D. R. Salahub and R. P. Messmer, *J. Chem. Phys.*, **64**, 2039 (1976).
(92) D. R. Salahub and R. P. Messmer, *Phys. Rev. B*, **14**, 2592 (1976).
(93) H. Köpf, *Angew. Chem., Int. Ed. Engl.*, **8**, 375 (1969).
(94) L. B. Clark, Ph.D. Thesis, University of Washington, 1963, quoted in ref 9.
(95) B. D. Sharma and J. Donohue, *Acta Crystallogr.*, **16**, 891 (1963).
(96) A. E. Foti, V. H. Smith, Jr., and J. W. D. Connolly, to be published.
(97) D. A. Lokben, T. W. Couch, and J. D. Corbett, Abstracts of the 160th National Meeting of the American Chemical Society, Chicago, Ill. 1970.

Ground- and Excited-State Correlations in Bond Rupture Reactions

E. M. Evleth* and E. Kassab

Contribution from the Centre de Mécanique Ondulatoire Appliquée, Paris 75019, France. Received June 5, 1978

Abstract: Semiempirically based molecular orbital configuration interaction ground- and excited-state correlation diagrams are generated for the bond ruptures in cyclobutane, water, ammonia, hydrogen peroxide, and hydrazine. All calculations confirm the topicity rules of Dauben, Salem, and Turro. It is shown, however, that the diagrams have some deceptive features with regard to correlations to Rydberg states.

Introduction

We will demonstrate that valence orbital level semiempirical self-consistent field configuration interaction (SCF–CI) calculation can be used to elucidate some of the correlative features of the potential energy surfaces for ground and excited singlet and triplet state bond rupture reactions. We will also analyze some of the deceptive features of such valence level correlations. The kinds of diagrams we will generate are the computational counterparts of the topicity rules formulated by Dauben, Salem, and Turro.[1]

We will deal specifically with certain cross sections of the surfaces for ruptures of CC, OO, NN, CN, NH, and OH single bonds. Although the calculation of all these surfaces is obtainable by current ab initio methods, only a few have been reported.[2] More importantly, it is common practice for various investigators to report only portions of surfaces for a few states of the molecule under study. Rarely is the reader given a total view of the interrelationships between various states of spectroscopic and/or photochemical interest and the ground state. We will attempt to do that here. The major goal of the work presented here is to confirm the topicity rules and to prepare the methodology for larger molecular systems for which good quality ab initio SCF–CI calculation of excited-state surfaces is presently too expensive. We have previously reported portions of the singlet surfaces on NH_3, N_2H_4,[3a] and H_2O_2.[3b]

Method of Calculation

A. Parametrization. The calculations presented here used the Eaker–Hinze parametrization for all bonds except CC and OO.[4] This parametrization retains most of the features of the CNDO/2 approximation but changes the resonance terms, β_{pq}, and the electron-other-core term, V_{ab}. In the CNDO/2 approximation, $V_{ab} = Z_b(aa|bb)$, Z_b is the core charge on atom b as seen by an electron in one of the orbitals on atom a, and $(aa|bb)$ is the two-centered electron–electron repulsion inte-

gral. The Eaker–Hinze approximation is (in atomic units)

$$V_{ab} = Z_b|(1 - \alpha)(aa|bb) + \alpha(R_{ab}^2 + 1/\dot\rho_a^2)^{-1/2}| \quad (1)$$

where R_{ab} is the distance between atoms a and b and ρ_a is the Slater orbital exponent for atom a. Eaker and Hinze found a best fit value for α of 0.3143 in calibrating their multiconfiguration (MCSCF) calculations to a number of physical observables. However, we found their parametrization not satisfactory for the OO bond energy in H_2O_2 (calcd, after CI, 155 kcal/mol; exptl, 51).[5] Likewise, their parametrization yielded a computed enthalpy for the cyclobutane → 2 ethylene reaction of about −70 kcal/mol (after 60 × 60 CI) whereas the experimental value is +18.[6] We chose to superimpose on the Eaker–Hinze parametrization that of Das Gupta and Huzinaga.[7]

$$V_{ab} = Z_b(1 + Be^{-CR_{ab}})(aa|bb) \quad (2)$$

For the case of the OO bond, $B = -0.069$, $C = 1$. For the CC bond $B = 1.294\,07$, $C = 1.872\,04$. In the case of carbon the resonance terms were also slightly modified: $\beta_{2s} = -0.5404$ au, $\beta_{2p} = -0.3985$.

It should be stressed that the use of either eq 1 or 2 is without theoretical justification. However, our parametrization, or that of the previous workers, does not differ from the classical CNDO/2 term for V_{ab} by more than 2% in the region where R_{ab} is greater than 1 Å.[8] Using this parametrization the OO bond in H_2O_2 has a dissociation energy of about 45 kcal/mol.[2b] The cyclobutane → 2 ethylene reaction has a calculated enthalpy of +4 kcal/mol at the 60 × 60 CI level. This latter value is deceptive because it is dependent on the amount of CI, becoming more exothermic as the level of CI is increased.[9] Likewise, the parametrization in H_2O_2 was not directly applicable to large-size peroxides. However, the use of eq 2 allows the enthalpy of a particular reaction to be calibrated to the experimental value after which the rest of the surface can be